

Measurement of tropospheric R O 2 and HO 2 radicals by a laser-induced fluorescence instrument

Hendrik Fuchs, Frank Holland, and Andreas Hofzumahaus

Citation: Review of Scientific Instruments 79, 084104 (2008); doi: 10.1063/1.2968712

View online: http://dx.doi.org/10.1063/1.2968712

View Table of Contents: http://scitation.aip.org/content/aip/journal/rsi/79/8?ver=pdfcov

Published by the AIP Publishing

Articles you may be interested in

The development and deployment of a ground-based, laser-induced fluorescence instrument for the in situ detection of iodine monoxide radicals

Rev. Sci. Instrum. 85, 044101 (2014); 10.1063/1.4869857

Note: A laser-flash photolysis and laser-induced fluorescence detection technique for measuring total HO2 reactivity in ambient air

Rev. Sci. Instrum. 84, 076106 (2013); 10.1063/1.4812634

A new photolysis laser-induced fluorescence instrument for the detection of H 2 O and HDO in the lower stratosphere

Rev. Sci. Instrum. 79, 064101 (2008); 10.1063/1.2940221

Development of a measurement system for nitrate radical and dinitrogen pentoxide using a thermal conversion/laser-induced fluorescence technique

Rev. Sci. Instrum. 76, 064101 (2005); 10.1063/1.1927098

A laser induced fluorescence instrument for measuring tropospheric NO 2

Rev. Sci. Instrum. 68, 4253 (1997); 10.1063/1.1148384



Measurement of tropospheric RO_2 and HO_2 radicals by a laser-induced fluorescence instrument

Hendrik Fuchs, ^{a)} Frank Holland, ^{b)} and Andreas Hofzumahaus^{c)} Forschungszentrum Jülich GmbH, Institut für Chemie und Dynamik der Geosphäre 2, 52425 Jülich, Germany

(Received 7 May 2008; accepted 17 July 2008; published online 26 August 2008)

A new method (ROxLIF) for the measurement of atmospheric peroxy radicals (HO₂ and RO₂) was developed using a two-step chemical conversion scheme and laser-induced fluorescence (LIF) for radical detection. Ambient air is sampled into a differentially pumped flow reactor, in which atmospheric RO_x radicals (=RO₂+RO+HO₂+OH) are chemically converted to HO₂ by a large excess of NO and CO at reduced pressures (ROx mode). When only CO is added as a reagent, the sum of atmospheric HO₂+OH is converted to HO₂ (HOx mode). At the reactor outlet, part of the air flow is transferred into a low-pressure detection chamber, where the HO₂ is further converted by reaction with NO to OH, which is then detected with high sensitivity by LIF at 308 nm. The ROxLIF technique has been implemented in an existing LIF instrument that is also capable of measuring atmospheric OH. From the concurrent measurements of RO_x, HO_x and OH, concentrations of HO₂ and RO₂ can be determined. The system is calibrated using the quantitative photolysis of water vapor at 185 nm as a radical source. Addition of CO or hydrocarbons to the calibration gas yields well-defined concentrations of HO2 or RO2, respectively, providing an estimated accuracy for the calibration of about 20%. The ROxLIF technique is extremely sensitive and has detection limits (signal-to-noise ratio=2) of about 0.1 pptv of HO₂ or RO₂ at a time resolution of 1 min. The paper describes the technique and its calibration, discusses the chemistry in the conversion reactor and possible interferences, and gives an example of ambient air measurements to demonstrate the performance of the new technique. © 2008 American Institute of Physics. [DOI: 10.1063/1.2968712]

I. INTRODUCTION

Hydroperoxy (HO₂) and organic peroxy (RO₂) radicals play an important role in the photochemical formation of tropospheric ozone and are chemically closely related to hydroxyl (OH) radicals, which constitute the major atmospheric oxidant. HO₂ and RO₂ are mainly produced by the reaction of OH with CO and volatile organic compounds, respectively:

$$CO + OH \rightarrow CO_2 + H, \tag{1}$$

$$H + O_2 + M \rightarrow HO_2 + M, \tag{2}$$

$$RH + OH \rightarrow R + H_2O,$$
 (3)

$$R + \mathcal{O}_2 + M \to R\mathcal{O}_2 + M, \tag{4}$$

here, RH denotes a hydrocarbon with R being an organic group and M refers to any third collision partner, mainly atmospheric N_2 or O_2 .

The main primary source of tropospheric OH is the reaction of water vapor with electronically excited $O(^1D)$ atoms which are produced by solar ultraviolet photolysis of O_3 :

$$O_3 + h\nu (<340 \text{ nm}) \rightarrow O(^1D) + O_2(^1\Delta, ^3\Sigma),$$
 (5)

$$O(^{1}D) + H_{2}O \rightarrow OH + OH.$$
 (6)

The main secondary source of OH is the chemical conversion of peroxy radicals by reactions with NO in the presence of high NO concentrations:

$$RO_2 + NO \rightarrow RO + NO_2,$$
 (7)

$$RO + O_2 \rightarrow R'O + HO_2,$$
 (8)

$$HO_2 + NO \rightarrow OH + NO_2.$$
 (9)

RO₂ is first converted to organic oxy radicals RO [reaction (7)], which undergo a very fast reaction with atmospheric O₂, forming HO₂ and carbonyl compounds R'O [reaction (8)]. HO₂ is then converted to OH by reaction with NO [reaction (9)]. As a result, the reaction sequence (7)–(9) recycles OH radicals which have been consumed by reactions (1) and (3). Thus, HO₂ and RO₂ reactions contribute significantly to the ability of OH to remove atmospheric pollutants.

Peroxy radicals are also essentially involved in the photochemical production of tropospheric ozone through photolysis of NO_2 which is produced by reactions (7) and (9):

a) Electronic mail: hendrik.fuchs@noaa.gov. Present address: NOAA Earth System Research Laboratory, Chemical Sciences Division, 325 Broadway, Boulder, CO 80305 and Cooperative Institute for Research in the Environmental Sciences, University of Colorado, Boulder, CO.

b)Electronic mail: f.holland@fz-juelich.de.

c) Electronic mail: a.hofzumahaus@fz-juelich.de.

$$NO_2 + h\nu (< 420 \text{ nm}) \rightarrow NO + O(^3P),$$
 (10)

$$O(^{3}P) + O_{2} + M \rightarrow O_{3} + M.$$
 (11)

The important role of peroxy radicals in atmospheric chemistry has motivated the development of measurement techniques for atmospheric RO_2 and HO_2 radicals. The detection methods that are currently applied do not distinguish speciated organic peroxy radicals but usually measure their sum. In this context it is useful to distinguish between RO_2 as the sum of all organic peroxy radicals in an air sample and RO_x which is the sum of $RO_2+RO+HO_x$. Here, RO is the total sum of oxy radicals and HO_x is the sum of $OO_2+RO_2+OO_3$.

The only existing technique for the direct and absolute measurement of tropospheric peroxy radicals is the matrix isolation and electron spin resonance spectroscopy (MI-ESR).^{3,4} Samples of ambient air are cryogenically collected and are later analyzed in the laboratory by ESR spectroscopy. The technique can specifically measure NO₂, NO₃, HO₂, and acetylperoxy radicals [CH₃C(O)O₂], as well as the sum of all other organic peroxy radicals. A detection limit of 1–2 pptv is achieved for a collection time of 30 min for each sample. However, the off-line analysis of one cryosample of air takes usually one laboratory day.

A widely applied measurement method for atmospheric peroxy radicals uses chemical amplification Peroxy Radical Chemical Amplifier (PERCA). 5-12 The PERCA technique actually measures RO_x , which is a good proxy for RO_2+HO_2 because atmospheric concentrations of RO and OH are much smaller than that of RO2+HO2. In a PERCA system, sampled ambient air is mixed with large concentrations of NO and CO. All RO₂ is converted into HO₂ [reactions (7) and (8), which then undergoes a chain reaction [reactions (1), (2), and (9)] in which HO₂ and OH are rapidly interconverted. The repetitive cycle between HO₂ and OH oxidizes NO to NO₂, which can reach a concentration up to 300 times larger than the initial concentration of RO₂+HO₂. The amplification by the chain length (CL) produces NO₂ concentrations that are sufficient to be routinely measured by a chemiluminescence detector, which uses the chemiluminescent reaction of NO₂ with luminol. Alternatively, Sadanaga et al. 10 developed a system in which the NO₂ concentration is measured by laser-induced fluorescence (LIF). PERCA instruments generally require calibration and can reach detection limits of a few pptv RO_x in a few minutes. Their sensitivity depends strongly on the water-vapor content of the air sample ^{13,14} for reasons that will be discussed later in Sec. VI.

Two chemical-ionization mass spectrometers (CIMSs) have been developed for measurement of atmospheric peroxy radicals, RO_x Chemical Conversion/CIMS, (ROxMAS)^{15,16} and Peroxy Radical Ionization Mass Spectrometer (PerCIMS).¹⁷ Both techniques apply chemical conversion and amplification like PERCAs but use SO_2 instead of CO for the conversion step of OH to HO_2 . The product H_2SO_4 , which is formed catalytically from the SO_2 oxidation by OH, is detected by CIMS. The high detection sensitivity of CIMS combined with amplification CLs of ~ 10 results in detection limits around 0.5 pptv peroxy radicals in 15–60 s measurement time. Both ROxMAS and PerCIMS are ca-

pable of distinguishing RO_2 and HO_2 by modulating the chemical conditions for the RO_2 to HO_2 conversion. In contrast to PERCA instruments, they exhibit no water-vapor dependence of the detection sensitivity for peroxy radicals.

LIF spectroscopy is a highly sensitive technique that is applied for the speciated measurement of tropospheric OH and HO₂ radicals. 18-23 In general, a continuous flow of ambient air is sampled by gas expansion into a low-pressure detection volume, where the OH radicals in the air flow are detected spectroscopically by LIF at 308 nm. Contrary, HO₂ radicals are not directly detectable by this technique. The radicals are first converted to OH by NO [reaction (9)], which is mixed into the gas expansion with a high concentration. Almost complete HO₂ conversion can be achieved so that this method measures the sum (HO_x) of ambient OH and HO₂. In order to distinguish between OH and HO₂ radical concentrations, OH is measured separately, for example, in a second fluorescence cell in which HO2 radicals are not converted to OH.²¹ Reported detection limits for this method are in the range of $(0.3-3) \times 10^6 \text{ HO}_2 \text{ radicals/cm}^3$ (corresponding to 0.01-0.1 pptv at 1 atm) at a time resolution of typically 1 min.²⁴

The low-pressure LIF instruments for measurement of HO_2 have no sensitivity to RO_2 . Although RO_2 is converted to RO by reaction (7) nearly as fast as HO₂ to OH [reaction (9)], the partial pressure of O_2 is generally too small in the low-pressure gas expansion to accomplish significant conversion of RO to OH by reactions (8) and (9) within the time required for the air flow to reach the laser beam for detection. In the current work, we have modified an existing lowpressure LIF instrument²¹ to enable also the efficient conversion of RO₂ to OH. The modified instrument can measure RO_x , HO_x , and OH concentrations with a high sensitivity yet without chemical amplification and allows the speciated determination of OH, HO2, and RO2 with a high time resolution. Here, we present the applied conversion technique for peroxy radicals and describe the instrumental characteristics and the calibration for different peroxy-radical species. An example of ambient air measurements demonstrates the performance of the new technique which is expected to provide improved understanding of the fast radical chemistry in the troposphere.

II. MEASUREMENT PRINCIPLE

Measurement of atmospheric peroxy radicals involves chemical conversion to OH in a two-stage process. In the first step RO_2 is converted to HO_2 inside a flow reactor at a reduced pressure. This is followed by further conversion to OH in a low-pressure chamber where OH is detected by LIF (Fig. 1).

A. Reactor chemistry

The ambient air that is to be analyzed is sampled at a flow rate of 7 slpm (slpm=liters per minute at 1 atm, 20 °C) through a 1 mm orifice into the flow reactor, which is differentially pumped and kept at a constant pressure of 25 hPa and room temperature. After the gas has passed the inlet nozzle, NO and CO are injected as reagent gases, yielding

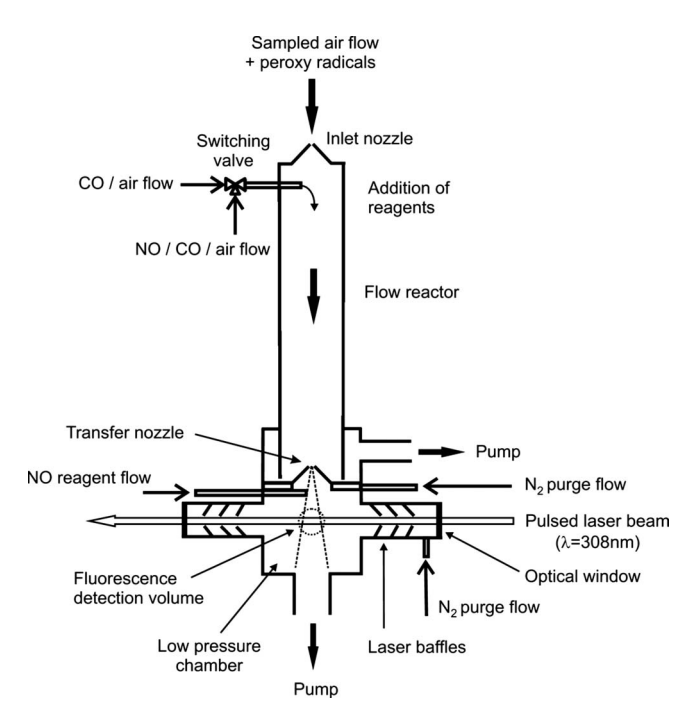


FIG. 1. Schematic of the RO_x measurement instrument. Sampled air is expanded into a low-pressure flow reactor at 25 hPa, in which RO_x radicals are converted into HO₂ by addition of NO and CO. At the exit of the reactor, part of the gas flow is transferred into a detection chamber at an even lower pressure (3.5 hPa), where HO₂ is converted into OH by excess NO. The OH is then detected by LIF at 308 nm. Details are given in the text.

mixing ratios of 0.7 ppmv NO and 0.17% CO in the sampled flow. The added NO initiates the successive conversion of RO_2 into RO, HO_2 , and OH via reactions (7)–(9) (Fig. 2) followed by rapid backreaction of OH with CO, yielding HO_2 [reactions (1) and (2)]. The high NO and CO concentrations force HO_2 and OH into a fast equilibrium, which is rate controlled by reactions (9) and (1). The equilibrium is reached within a few milliseconds with a partitioning ratio $[HO_2]/[OH]=k_1[CO]/k_9[NO]$ of about 50 at the given con-

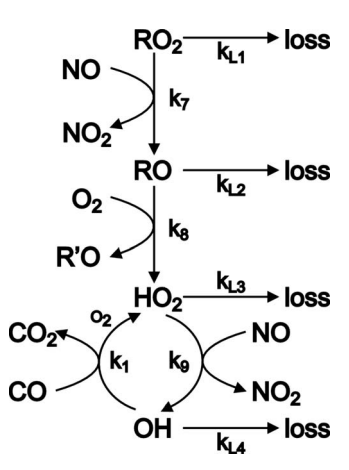


FIG. 2. Simplified chemical scheme of the successive conversion of organic peroxy radicals RO_2 to RO, HO_2 and OH radicals. k_i (i=1,7–9) denote the bimolecular rate constants for the corresponding radical reactions (see text). Each radical species can undergo additional loss reactions by gas-phase recombination with NO or by collisions with the reactor walls. The corresponding loss-rate coefficients k_{L1} and k_{L2} are defined by Eqs. (31) and (34), respectively. In a similar way, k_{L3} and k_{L4} can be defined for losses of HO_2 [reactions (16) and (17)] and OH [reactions (18) and (19)], respectively. R'O represents organic carbonyl compounds.

TABLE I. Reactor chemistry: Reactions and rate constants at 25 hPa and 298 K.

Reaction	$k \text{ (cm}^3 \text{ s}^{-1})$			
$OH+CO\rightarrow CO_2+H$	1.5×10 ^{-13 a}			
$OH+NO+M \rightarrow HONO+M$	3.8×10^{-13} a			
$OH + NO_2 + M \rightarrow HONO_2 + M$	9.8×10^{-13} a			
$OH+HO_2 \rightarrow H_2O+O_2$	1.1×10^{-10} a			
$OH+wall \rightarrow products$	5.4 ^b , c			
$H+O_2+M \rightarrow HO_2+M$	3.4×10^{-14} a			
$HO_2+NO \rightarrow OH+NO_2$	8.1×10^{-12} a			
$HO_2+NO+M \rightarrow HONO_2+M$	2.4×10^{-15} d,e			
$HO_2 + NO_2 + M \rightarrow HO_2NO_2 + M$	9.5×10^{-14} a			
$HO_2 + HO_2(+M) \rightarrow H_2O_2 + O_2(+M)$	1.7×10^{-12} a,e			
HO_2 + wall \rightarrow products	0.5 ^{b,c}			
$R = CH_3$				
$CH_3O_2 + NO \rightarrow CH_3O + NO_2$	7.7×10^{-12} a			
$CH_3O_2 + NO + M \rightarrow CH_3ONO_2 + M$	6×10^{-14} f			
$CH_3O_2 + NO_2 + M \rightarrow CH_3O_2NO_2 + M$	6.1×10^{-13} a			
$CH_3O_2 + HO_2 \rightarrow CH_3OOH + O_2$	5.2×10^{-12} a			
$CH_3O_2 + CH_3O_2 \rightarrow products$	3.5×10^{-13} a			
CH_3O_2 +wall \rightarrow products	$0.15^{b,g}$			
$CH_3O+O_2 \rightarrow CH_2O+HO_2$	1.9×10^{-15} a			
$CH_3O+NO+M \rightarrow CH_3ONO+M$	4.9×10^{-12} a			
$CH_3O + NO_2 + M \rightarrow CH_3ONO_2 + M$	7.5×10^{-12} a			
$CH_3O + wall \rightarrow product$	5.4 ^{b,h}			
$R = C_n H_{2n+1}$ ($n \ge 2$; from alkanes + OH)				
$RO_2 + NO \rightarrow RO + NO_2$	9.0×10^{-12} i			
$RO_2 + NO + M \rightarrow RONO_2 + M$	$<9.0 \times 10^{-13}$ f,j			
$RO_2 + NO_2 + M \rightarrow RO_2NO_2 + M$	2.5×10^{-12} a,k			
$RO_2 + HO_2 \rightarrow ROOH + O_2$	8.0×10^{-12} a,k			
RO_2 + wall \rightarrow products	$0.15^{b,g}$			
$RO + O_2 \rightarrow R'O + HO_2$	$\sim 1 \times 10^{-14}$			
$RO + NO + M \rightarrow RONO + M$	4.2×10^{-11} a,k			
$RO + NO_2 + M \rightarrow RONO_2 + M$	2.4×10^{-11} a,k			
RO + wall \rightarrow products	5.4 ^{b,h}			
$R = CH_2(OH)CH_2$ (from ethene+OH)				
$RO_2 + NO \rightarrow RO + NO_2$ 9×10^{-12} m				
$R = C_5 H_8(OH)$ (from isoprene+OH)				
$RO_2 + NO \rightarrow RO + NO_2$	9×10^{-12} n			

^aNASA-JPL recommendation by Sander *et al.* (Ref 48). In the case of termolecular reactions, pseudo-second-order rate coefficients are given.

ditions (rate constant values are given in Table I). As a result, the reactor chemistry converts RO_2 effectively into HO_x which almost entirely consists of HO_2 , the much less reactive member of the HO_x family.

The rate of the RO_2 to HO_2 conversion is limited by

^bFirst-order rate coefficient (s^{-1}) .

^cMeasured in this work.

^dEstimate based on measured results by Butkovskaya et al. (Ref. 39).

^eAssuming 1% water vapor.

^fEstimate using the parametrized pressure dependence of Zhang *et al.* (Ref. 53).

^gEstimate using the measured ratio $k(RO_2+wall)/k(HO_2+wall)=0.3$ from Mihele and Hastie (Ref. 37).

^hAssumption: $k(RO+wall) \approx k(OH+wall)$.

ⁱReview by Atkinson and Arey (Ref. 1).

 $^{^{\}rm j}k$ increases approximately linearly with carbon number from 1.3 \times 10⁻¹³ (n=2) to 9×10⁻¹³ cm³ s⁻¹(n=8).

 $^{^{}k}$ For n=2.

 $^{^{1}}k\sim9.5\times10^{-15}$ cm³ s⁻¹ for primary (*R*CH₂O) and $\sim8\times10^{-15}$ cm³ s⁻¹ for secondary (*RR*'CHO) radicals, recommended by Atkinson (Ref. 40).

^mReview by Atkinson (Ref. 40).

ⁿMeasurement by Zhang et al. (Ref. 43).

reaction (7), yielding a pseudo-first-order decay of RO_2 with a lifetime of 0.3 s at the given conditions. Thus, RO_2 is almost completely converted in the reactor, in which the sampled air flow has a mean residence time of 0.6 s. The overall yield of HO_2 , however, is diminished by radical losses. First of all, RO_2 and RO can undergo termolecular recombination reactions with the added NO:

$$RO_2 + NO + M \rightarrow RONO_2 + M,$$
 (12)

$$RO + NO + M \rightarrow RONO + M,$$
 (13)

or can be lost by reactive collisions with the Teflon surface of the reactor walls:

$$RO_2$$
 + wall \rightarrow products, (14)

$$RO + wall \rightarrow products.$$
 (15)

The pressure-dependent reactions with NO are relatively slow at the low reactor pressure and are of similar rate or even slower than those of the corresponding wall loss reactions (Table I). Reactions (12)–(15) reduce the HO_2 yield from RO_2 conversion only in the order of a few percent (see Sec. IV for details).

 HO_2 radicals undergo similar types of loss reactions as RO_2 :

$$HO_2 + NO + M \rightarrow HONO_2 + M,$$
 (16)

$$HO_2 + wall \rightarrow products.$$
 (17)

Both reactions are relatively slow at the given conditions. The wall reaction is the dominating loss process, which reduces the total HO_2 yield in the order of 20% (see Sec. VI).

OH radicals formed in the reactor by reaction (9) undergo similar loss reactions as RO:

$$OH + NO + M \rightarrow HONO + M,$$
 (18)

$$OH + wall \rightarrow products.$$
 (19)

These two reactions compete with the reaction of OH with CO, which is much faster owing to the large amount of added CO. Thus, HO_x radical losses via reactions (18) and (19) become negligible.

As a result of the reactor chemistry, all RO_x species (i.e., RO_2 , RO, HO_2 , and OH) become eventually HO_2 at the exit of the flow reactor. This is also the case for atmospheric RO, HO_2 , and OH radicals which are collected through the inlet nozzle of the reactor. This measurement mode, in which NO and CO are added as reagent gases, is therefore called the "ROx mode." If the NO addition is turned off and only CO is added as reagent and if the mixing ratio of NO in the sampled ambient air is sufficiently small (<25 ppbv), the conversion of RO_2 to HO_2 is negligible. The reactor converts only atmospheric RO, HO_2 , and OH into HO_2 under these conditions. Since the ambient RO concentration is very small and makes a negligible contribution, this measurement mode is called the "HOx mode."

B. HO₂ conversion and LIF detection

At the exit of the flow reactor, the central part of the flow is drawn through a transfer nozzle into the detection chamber, which is kept at an even lower pressure (3.5 hPa). Additional NO is injected into the emerging gas expansion, raising the NO mixing ratio to about 300 ppmv. The high excess of NO shifts the equilibrium between HO₂ and OH to OH, which is detected further downstream by LIF at 308 nm. The radical detection is performed essentially in the same way as described by Holland et al. 20,25 Briefly, a pulsed narrowbandwidth UV laser is used to excite the OH radicals on a single rovibronic transition, for example, on the $Q_1(3)$ line of the $A^2\Sigma^+v'=0-X^2\Pi v''=0$ transition, and the resulting resonance fluorescence is measured by gated photon counting using a time delay to discriminate the longer-lived OH fluorescence ($\tau_{\text{fluoresc}} \approx 150 \text{ ns at } 3.5 \text{ hPa}$) from the instantaneous laser stray light (approximately 20 ns duration). Furthermore, the laser is tuned periodically on and off resonance to distinguish the OH fluorescence signal from any nonresonant background signals. The amount of detected OH fluorescence integrated for typically 30 s over successive laser pulses is taken as a measure of the radical concentration. The conversion of the fluorescence signals into ambient radical concentration requires a calibration as explained in Sec. IV.

III. EXPERIMENTAL

The instrument consists essentially of the LIF setup that has been used previously for simultaneous measurements of OH and HO₂ in field campaigns²⁵ and in experiments at the outdoor simulation chamber SAPHIR in Jülich, Germany.²⁶ Some modifications have been implemented. The existing detection chamber for HO2 radicals was extended into the RO_r measurement device outlined above (Fig. 1), while another detection chamber remains available for OH. Thus, simultaneous measurements of OH can be performed along with alternating RO_x and HO_x measurements. The other major change in the LIF instrument is the replacement of the UV generating laser system. In the following only the major modifications will be described, whereas a description of the basic instrument can be found elsewhere. 20,21,25 Important parameters of the new RO_x measurement device are summarized in Table II.

A. Flow reactor

The flow reactor for chemical RO_x conversion is a cylindrical aluminum tube which is internally covered by a Teflon surface to minimize wall loss reactions. The reactor has an internal diameter of 66 mm and a length of 830 mm. The top flange of the reactor carries an inlet nozzle (Beam Dynamics, nickel, opening angle of 70°, orifice of 1 mm), which transmits an air flow of 7 slpm when the reactor is operated at a pressure of 25 hPa. Half of the gas flow is drawn into the LIF detection chamber, while the excess gas is removed by an oil-free vacuum pump (Edwards, XDS35i). The pressure in the reactor is stabilized by a motorized throttle valve (MKS, type 153) mounted on the inlet of the vacuum pump. The reagent gases are introduced as gas mixtures (Linde AG) with concentrations of 500 ppmv NO (99.5%) in N_2 (99.9990%) and 10% CO (99.997%) in N_2 (99.9990%) through a glass tube (4 mm inner diameter), which ends in the center of the reactor tube about 20 mm downstream of

TABLE II. Experimental parameters of the ROxLIF Instrument

	Parameter	Value
Flow reactor	Inlet nozzle orifice	1.0 mm
	Sample flow rate	7 slpm ^a
	Reagent mixing ratio (after addition)	0.7 ppmv NO, 0.17% CO
	Geometry (length × diameter)	830×66 mm
	Volume	2.81
	Pressure	25 hPa
	Temperature	Room temperature
	Flow residence time	0.62 s
Fluorescence cell	Transfer nozzle orifice	4.0 mm
	Sample flow rate	3.5 slpm ^a
	Reagent mixing ratio (after addition)	300 ppmv NO
	Pressure	3.5 hPa
	Laser power (308 nm)	25 mW (typically)
	Laser repetition rate	8.55 kHz
	Laser pulse length (full width at half maximum)	20 ns
	Laser beam diameter	8 mm
	Photon-counter gate delay	70 ns
	Photon-counter gate duration	500 ns

^aslpm=liter per minute at 1 atm, 20 °C.

the inlet nozzle. The added gas flows of 10 sccm NO mixture and 120 sccm CO mixture (sccm denotes cubic centimeter per minute at 1 atm, 20° C) are controlled by mass flow controllers (Brooks, 5850TR).

B. LIF detection

The LIF detection chamber is equipped with a homemade conically shaped inlet nozzle (stainless steel, opening angle of 70°, orifice of 4 mm), which transmits 3.5 slpm of air from the reactor. The expanding gas beam is embedded in a purge flow of 1 slpm of clean nitrogen (99.9990%, Linde AG). For the chemical HO₂ conversion, about 1 sccm of pure NO (99.5%, Linde AG), controlled by a mass flow controller, is injected into the gas expansion, after the NO flow has passed a cartridge filled with ascarite (Sigma–Aldrich) for additional purification. The pressure in the LIF detection chamber is regulated by another control valve (MKS, type 153) that is placed in front of a dry vacuum pump (Edwards, IPX 500).

The OH radicals from the $\rm HO_2$ conversion are excited by a pulsed laser beam (8 mm diameter) that crosses perpendicular to the gas flow at the center of the fluorescence chamber. The laser system consists of a frequency-doubled neodymium doped yttrium aluminum garnet laser (Photonics, DS20, 8.5 W output power at 532 nm) which pumps a wavelength-tunable narrow-bandwidth dye laser (Laser Analytical Systems, Intradye). Using a dye solution of 80 mg/l rhodamine 101 in ethanol, up to 1 W output power is achieved at 616.3 nm, which is externally frequency doubled (second harmonic generation) to 308.15 nm by a β -Barium Borate (BBO) crystal. The maximum UV laser power is 80 mW at a repetition rate of 8.5 kHz and a pulse width of 20 ns, but only 25 mW is normally used for detection to avoid saturation of the OH-line transition.

IV. CALIBRATION

A radical source which was developed for calibration of OH and HO_2 measurements is used for calibration of the $R\mathrm{O}_x$ measurement device. The method is based on the concept of HO_x generation by water-vapor photolysis in air at 1 atm using the 185 nm radiation from a low-pressure discharge mercury lamp. Equal amounts of OH and HO_2 radicals are produced by this process:

$$H_2O + h\nu \rightarrow OH + H,$$

$$H + O_2 + M \rightarrow HO_2 + M. \tag{20}$$

The absolute radical concentration provided by the calibration source can be related to the amount of ozone that is simultaneously formed by the photolysis of oxygen at 185 nm in the air flow:^{27,29}

$$O_2 + h\nu \rightarrow O + O$$
,
 $O + O_2 + M \rightarrow O_3 + M$. (21)

The radical concentrations are then determined by the equation

$$[OH]_0 = [HO_2]_0 = \frac{\sigma_{H_2O}[H_2O]}{2\sigma_{O_2}[O_2]}[O_3],$$
 (22)

where O_3 and H_2O concentrations can be measured. The absorption cross section of water vapor at 185 nm, $\sigma_{H_2O} = (7.1 \pm 0.2) \times 10^{-20}$ cm², is taken from the literature. The lamp-specific effective cross section of oxygen is from our laboratory measurements and has a value of $\sigma_{O_2} = (1.28 \pm 0.05) \times 10^{-20}$ cm². 25,30

The radical source can be operated to provide only $\rm HO_2$ radicals by adding CO to the synthetic air for complete conversion of OH to $\rm HO_2$ [reactions (1) and (2)]. This way the source provides $\rm HO_2$ radicals with a quantum yield of 2. In a

similar way, specific RO_2 radicals can be generated by scavenging all OH radicals with a suitable hydrocarbon [reactions (3) and (4)]. In this case the source yields equal concentrations of RO_2 and HO_2 , i.e., $[RO_2]_0 = [HO_2]_0$. As a constraint, it is required that the hydrocarbon is not significantly photolyzed at 185 nm.

The calibration is performed by running a fast laminar flow of humidified synthetic air (Linde AG, purity of 99.995%) with a possible admixture of CO or a hydrocarbon through a cylindrical quartz tube. A short distance upstream of the tube outlet, the gas mixture is irradiated by collimated 185 nm radiation, which is transmitted perpendicular through the quartz tube. The photolytically generated radicals are transported by the gas flow to the inlet nozzle of the RO_x conversion reactor, which sticks concentrically into the outlet opening of the quartz tube. The amount of CO or hydrocarbon, which is optionally added, is chosen to achieve complete OH conversion within the transport time $(\approx 20 \text{ ms})$ before the calibration gas enters the LIF instrument. A typical mixing ratio of 0.15% of CH₄ is applied for generation of CH₃O₂, while equivalent concentrations of the same OH reactivity are used for other hydrocarbons. In each case, the hydrocarbon concentration is sufficiently small that it does not disturb the chemical HO₂ to HO₂ conversion that takes place inside the RO_x reactor.

The detection sensitivities C_i of the measurement system for the different radical species ($i=RO_x$, HO_2 , and OH) can be determined from a combination of measurements using gas from the calibration source (1) with added CO, (2) with added RH, and (3) without any reactant:

$$S_1 = 2C_{\text{HO}_2}[\text{HO}_2]_0,$$
 (23)

$$S_2 = C_{\text{HO}_2}[\text{HO}_2]_0 + C_{\text{RO}_2}[RO_2]_0$$
 (24)

$$S_3 = C_{\text{HO}_2}[\text{HO}_2]_0 + C_{\text{OH}}[\text{OH}]_0.$$
 (25)

The sensitivity C_i for each species is given by the fluorescence photon count rate (counts/s) per number density (cm⁻³) of the respective radical in the sampled air and per milliwatt of UV laser power. S_j (j=1-3) denotes the measured corresponding fluorescence signals. The sensitivities can then be determined as

$$C_{\text{HO}_2} = \frac{S_1}{2[\text{HO}_2]_0} \tag{26}$$

$$C_{RO_2} = \frac{S_2}{[RO_2]_0} - C_{HO_2} \tag{27}$$

$$C_{\text{OH}} = \frac{S_3}{2[\text{OH}]_0} - C_{\text{HO}_2}$$
 (28)

V. DETECTION SENSITIVITY MODEL

In order to get an understanding of the RO_x detection sensitivity, a model of the flow-reactor chemistry is useful. Chemical reactions that may play a role in the reactor are listed in Table I. A closer inspection shows that the reactor chemistry can be described by a relatively simple kinetic

model for the present instrumental conditions (Table II). One reason for the simplification is the large excess of reagent gases (CO, NO), which controls the radical chemistry (see Sec. II). Another reason is the low pressure in the reactor, which slows down unwanted radical reactions so that they become mostly negligible. This is the case for (1) radical losses that occur by pressure-dependent recombination reactions of RO_x species with added NO, (2) radical-radical reactions, and (3) radical reactions with reactive species (e.g., NO_2) from ambient air.

As was explained in Sec. II, atmospheric HO_x and RO radicals are converted immediately, i.e., in a few milliseconds, into HO_2 in the flow reactor, where HO_2 radicals are partially lost by wall reaction, while they are transported to the reactor exit. On the time scale of the transportation time (0.6 s) the expected time-dependent decay can be approximated by

$$[HO_2]_a(t) = ([HO_x]_0 + [RO]_0)e^{-k_{17}t},$$
 (29)

where $[HO_x]_0$ and $[RO]_0$ are the concentrations of atmospheric HO_x and RO, respectively, entering the reactor and t is the reaction time. Index a denotes that the HO_2 comes from HO_x and RO conversion.

Atmospheric RO_2 radicals that come into the flow reactor are chemically converted by the large excess of added NO or are destroyed at the reactor wall. Here, the time-dependent decay of RO_2 can be described as

$$[RO_2](t) = [RO_2]_0 e^{-(k_7[NO] + k_{L1})t},$$
 (30)

where $[RO_2]_0$ is the initial RO_2 concentration and k_{L1} is the first-order rate coefficient for the loss processes that remove RO_2 without producing new radicals:

$$k_{L1} = k_{12}[NO][M] + k_{14}.$$
 (31)

The conversion of RO_2 to HO_2 via reactions (7) and (8) is rate limited by reaction (7) and occurs with an overall yield of $\alpha_{RO_2}\alpha_{RO}$, giving the net reaction

$$RO_2 + NO \rightarrow \alpha_{RO_2} \alpha_{RO} HO_2.$$
 (32)

 α_{RO_2} and α_{RO} can be calculated from the branching ratios for reactions (7) and (8) in competition with the corresponding radical loss reactions, respectively (see Fig. 2):

$$\alpha_{RO_2} = \frac{k_7[NO]}{k_7[NO] + k_{L1}}$$
 and $\alpha_{RO} = \frac{k_8[O_2]}{k_8[O_2] + k_{L2}}$, (33)

with

$$k_{12} = k_{13}[NO][M] + k_{15}.$$
 (34)

This implies that the HO_2 kinetics is mainly controlled by two processes: (1) the production via net reaction (32) and (2) the destruction by wall reaction (17). Accordingly, the time dependence of the HO_2 concentration assumes the functional form of a simple consecutive mechanism:

$$[HO_{2}]_{b}(t) = [RO_{2}]_{0} \frac{\alpha_{RO_{2}} \alpha_{RO} k_{7}[NO]}{k_{17} - (k_{7}[NO] + k_{L1})} \times (e^{-(k_{7}[NO] + k_{L1})t} - e^{-k_{17}t}).$$
(35)

Here, index b denotes that the HO_2 comes from RO_2 conversion. In atmospheric measurements of RO_x , the HO_2 concen-

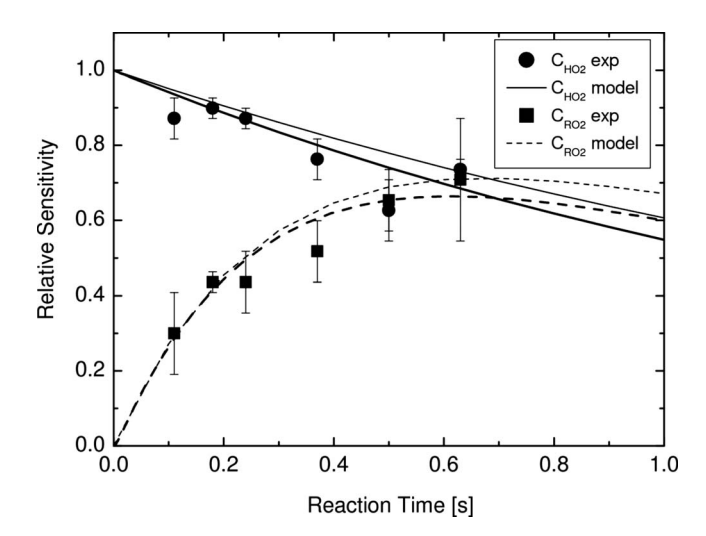


FIG. 3. Relative detection sensitivities for HO_2 and CH_3O_2 as a function of the gas residence time in the flow reactor. The symbols show the experimental dependence which was obtained by varying the length of the reactor at otherwise constant conditions. Error bars are 1σ standard deviations of the measurements. The solid and dashed lines represent chemical model simulations. The thick lines use a full model; the thin lines apply the analytical expressions of Eqs. (29) and (35) (see text).

tration at the exit of the flow reactor is then given by

$$[HO_2](t_r) = [HO_2]_a(t_r) + [HO_2]_b(t_r),$$
 (36)

where t_r is the gas residence time in the reactor.

In the LIF detection chamber the detection sensitivity of HO_2 is independent of the admixture of CO and NO introduced in the flow reactor. The concentrations of these reagents are so small that they influence neither the HO_2 to OH conversion in the chamber nor the fluorescence quenching of the excited OH radicals. Thus, Eq. (36) provides a relative measure of the expected detection sensitivity for atmospheric peroxy radicals as a function of the chemical reactor conditions. In the following, we will use the ratios $[HO_2]_a/[HO_2]_0$ from Eq. (29) and $[HO_2]_b/[RO_2]_0$ from Eq. (35) as a model to study the influence of the reactor conditions on the relative detection sensitivities for atmospheric HO_2 and RO_2 , respectively.

VI. INSTRUMENTAL CHARACTERIZATION

A. Reaction-time dependence

Relative detection sensitivities for HO_2 and CH_3O_2 were measured as a function of the gas residence time in the flow reactor, operating the LIF instrument in the RO_x measurement mode (Fig. 3). The measurements were obtained by varying the length of the RO_x reactor at otherwise constant conditions (see Table II), using the calibration device as a radical source. The sensitivity for HO_2 was found to decrease continuously with reaction time, whereas the sensitivity for CH_3O_2 first increases and then levels off after 0.6 s. The experimentally observed behavior is well reproduced by model simulations, using either the full chemical mechanism from Table I or the simple analytical approach represented by Eqs. (29) and (35). The full model predicts slightly lower

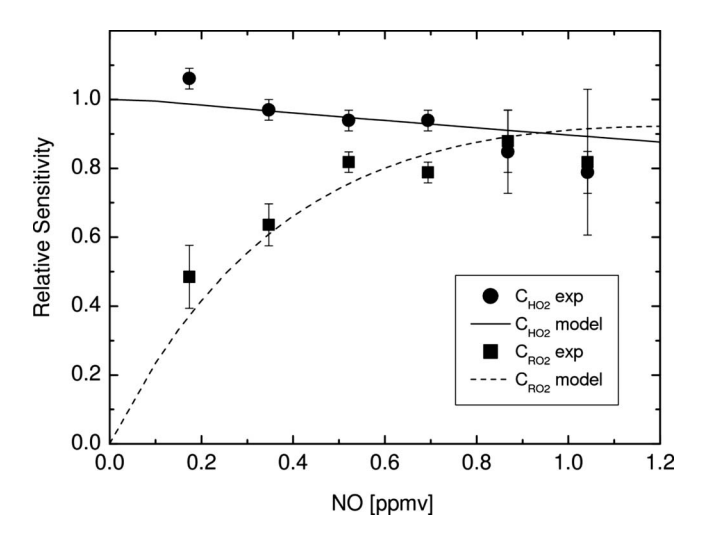


FIG. 4. Relative detection sensitivities for HO_2 and CH_3O_2 as a function of the NO mixing ratio in the flow reactor. The symbols show the experimental dependence. Error bars are 1σ standard deviations of the measurements. The solid and dashed lines represent simulations with the full chemical model (see text).

sensitivities than the analytical model. The difference can be explained by HO_x losses caused by OH wall reaction, which is neglected in the analytical approach.

According to the analytical model, 74% of the initial HO_2 radicals are transmitted through the reactor for the normally chosen residence time of 0.6 s, while 26% is lost by wall reaction. 87% of the initial CH_3O_2 radicals are consumed in the reactor, but only 63% of the organic radicals yield HO_2 at the exit of the flow reactor. The difference is mainly caused by wall reactions of CH_3O_2 $(1-\alpha_{RO_2}=5\%)$, CH_3O $(1-\alpha_{RO}=3\%)$, and HO_2 (16%). Gas-phase losses by termolecular reactions with NO [reactions (16), (12), and (13)] are negligible (<1%).

B. HO_x wall reactions

The rate coefficients for the wall reactions of OH and HO₂, which are used in the model calculations, were measured similarly as in the case of Fig. 3 but without addition of reagent gases (NO, CO) in the reactor. The HO₂ loss rate was determined while the calibration device was operated as a pure HO₂ source. For measurement of the OH loss rate, the calibration device provided OH with equal amounts of HO₂, but the NO addition in the LIF detection chamber was switched off to avoid detection of HO₂. The rate coefficient for OH (5.4 s⁻¹) was found to be ten times faster than that for HO_2 (0.5 s⁻¹). The difference cannot be explained by different transport rates of the two radical species to the wall because the diffusion coefficients [OH: 0.22 atm cm² s⁻¹; HO_2 : 0.14 atm cm² s⁻¹ (Ref. 33)] are too similar. It can be rather explained by a different wall-reaction probability, which was measured to be ten times larger for OH compared to that for HO₂ for reaction on a Teflon surface.³⁴

C. NO dependence

The relative NO dependence of the detection sensitivities was tested for otherwise normal operating conditions of the instrument. Figure 4 shows the experimental dependence together with the prediction of the full model simulation. A weak NO dependence is found for HO_2 in both measurement and model. A decrease in the HO_2 detection sensitivity by about 8% is inferred from the model when the NO mixing ratio is increased from zero to 0.7 ppmv. This can be explained by an increase in the $\mathrm{OH/HO}_2$ ratio from zero to about 0.02, respectively, resulting in a small but increasing loss of HO_x through OH wall reaction. Note that the same effect causes the difference between the two model curves of C_{HO_2} in Fig. 3.

In the case of CH_3O_2 , the sensitivity increases with the NO mixing ratio, as is expected, and reaches a broad maximum above 0.6 ppmv NO. Figure 4 demonstrates that the detection of HO_2 and CH_3O_2 has little sensitivity to variations in NO at the standard condition of 0.7 ppmv NO.

D. Water-vapor dependence

Water vapor can potentially interfere with the radical detection in various ways. First, it is well known that laser-induced OH fluorescence is efficiently quenched by $\rm H_2O$, thus influencing the sensitivity of OH detection. Under particular circumstances, i.e., in a very cold adiabatic gas expansion, additional loss of OH fluorescence signal has been observed at high humidity. The effect, in the order of a factor 2, was attributed to undetected OH which was probably taken up by clustering water molecules. Eurthermore, it has been reported that chemical amplifiers for measurement of RO_2 show a strong change in detection sensitivity (up to a factor of 2–3) caused by water-vapor enhanced radical losses. 13,14,37

The water-vapor influence on the ROxLIF instrument was investigated using the calibration source to provide peroxy radicals in synthetic air at different mixing ratios of H₂O. The detection sensitivities for HO₂ and CH₃O₂ were found to decrease by 10% over the range of 0%–1% of water vapor, with the same functional dependence for both radical species (Fig. 5). This observation can be well described by a model that accounts for OH fluorescence quenching by H₂O in the LIF detection. The model (represented by the solid lines in Fig. 5) makes use of a theoretical description of laser-induced OH fluorescence detection²⁰ and applies rate coefficients for quenching of OH(A ${}^{2}\Sigma^{+}, v=0$) compiled by Heard and Henderson.³⁸ The good agreement of experiment and model rules out the significance of other effects. This conclusion can be supported by further arguments. First, the LIF detection in the present instrument occurs in a warm gas expansion at room temperature, for which signal loss by radical uptake in water clusters has not been observed.²

Furthermore, the strong water-vapor dependence observed for PERCAs is not expected for ROxLIF, although both techniques use similar chemistry for the conversion of RO_2 . Part of the water-vapor dependence of PERCA instruments has been attributed to enhanced radical losses on wall surfaces.³⁷ It was observed that the wall reactivity of HO_2 in air in a Teflon tube at atmospheric pressure increased by a factor of 2 for an increase in relative humidity from zero to 50%, while the wall loss of RO_2 was constant. In our instrument, the water-vapor concentration and the likelihood of water layer on the wall surface are strongly diminished be-

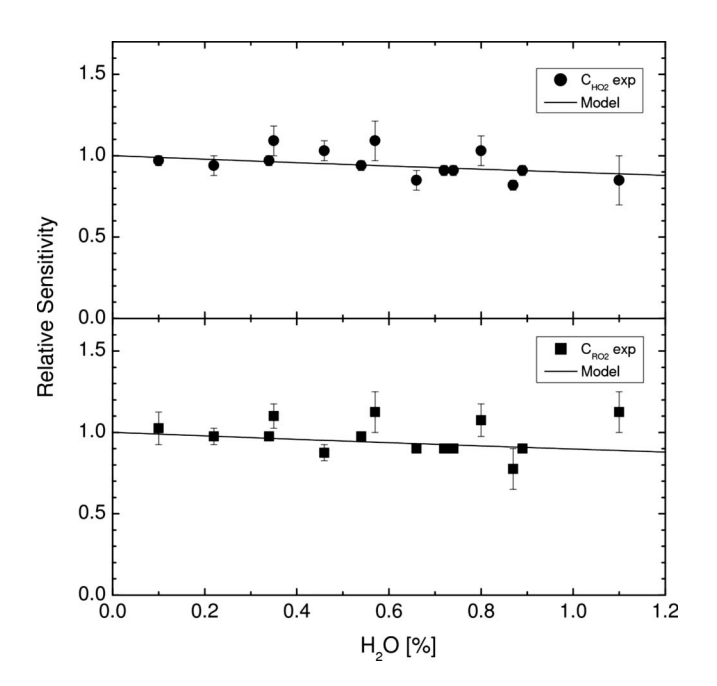


FIG. 5. Relative detection sensitivities for HO_2 and CH_3O_2 as a function of the H_2O mixing ratio in the sampled air. The symbols represent experimental data. The solid lines display the theoretical dependence expected from the OH fluorescence quenching by gaseous water. Error bars are 1σ standard deviations of the measurements.

cause the total pressure is reduced by a factor of 40. Thus, an enhancement in HO_2 wall losses by water vapor is unlikely to play a role, in agreement with the findings shown in Fig. 5.

Another part of the water-vapor dependence of PERCA instruments has been attributed to a small radical loss $(\approx 1\%)$ in the interconversion of HO_x, which is greatly amplified through repetitive HO_x cycling. 14,37 A suggested gasphase mechanism, which agrees quantitatively with the recent kinetic study by Butkovskaya et al.,39 is the reaction of HO₂·H₂O adducts with NO, leading to HNO₃ as a nonradical product rather than OH+NO2. This possible reaction channel is slowed down in our instrument by more than an order of magnitude because of the reduced reactor pressure, which decreases the number densities of H₂O and accordingly of the HO₂·H₂O adducts. Furthermore, the ROxLIF technique requires no amplification because of the high detection sensitivity of LIF. The effective CL can be estimated from the amount of NO₂ that is expected from the HO₂ +NO reaction in the flow reactor,

$$CL = \frac{\Delta[NO_2]}{[RO_2]_0} = k_9[NO] \int_0^{t_r} [HO_2]_b(t) dt,$$
 (37)

yielding a value of $CL \approx 1$. The low pressure in the reactor leads to reduced number densities of added reactants so that the chemical conversion of peroxy radicals is slow compared to their conversion at atmospheric pressure. Thus, the CL is short and any kind of radical loss in the HO_x cycling is not amplified.

E. Detection sensitivities

The RO_x instrument was absolutely calibrated for different radical species. The sensitivity C_i for each species is

TABLE III. Measured relative sensitivity of the ROxLIF instrument for different RO₂.

Hydrocarbon	Peroxy radicals ^a	Relative sensitivity ^b , ^c
Methane	CH_3O_2	1.00 ± 0.05
Ethane	$CH_3CH_2O_2$	0.91 ± 0.03
Propane	$C_2H_5CH_2O_2$, $(CH_3)_2CHO_2$	0.96 ± 0.04
Isobutane	(CH ₃) ₃ CO ₂ , (CH ₃) ₂ CHCH ₂ O ₂	0.59 ± 0.04
Ethene	CH ₂ (OH)CH ₂ O ₂	0.98 ± 0.05
Isoprene	$C_5H_8(OH)O_2^{-d}$	1.21 ± 0.06

^aFrom hydrocarbon reaction with OH.

given by the fluorescence photon count rate (counts/s) per number density (cm⁻³) of the respective radical in the sampled air and per milliwatt of UV laser power. A value of 1.2×10^{-7} counts s⁻¹ cm³ mW⁻¹ was determined for HO₂, with an estimated uncertainty of $\pm 20\%$ (2σ) resulting from the applied calibration method.²⁵ The detection sensitivities for CH₃O₂ and OH were found to differ from those of HO₂, with $C_{\text{CH}_3\text{O}_2}$: C_{HO_2} : C_{OH} =1.2:1.0:0.72, while the model calculates almost the same values for the three radical types. The smaller detection sensitivity for HO₂ and OH, relative to that for CH₃O₂, is probably caused by losses in the inlet region of the reactor, before the reagent gases are added and completely mixed, and reflects the general higher reactivity of these radicals.

In order to apply the instrument for atmospheric measurements, it is also important to understand how the instrument responds to different RO_2 species. Various organic peroxy radicals were generated by reaction of OH with methane, ethane, propane, isobutane, ethene, and isoprene. The measured sensitivities for the resulting peroxy radicals were normalized to the CH_3O_2 sensitivity and are listed in Table III. The values for the peroxy radicals from the OH reaction with methane, ethane, propane, and ethene are similar within 10%. The result for the hydroxyalkyl peroxy radicals from isoprene+OH is slightly larger (+20%), whereas the result for the peroxy radicals from isobutane+OH is substantially lower (-40%).

The similarity of the experimental values for the peroxy radicals from the three n-alkanes (C_1 - C_3) is consistent with the known chemistry. Using the analytical model [Eq. (35)], the predicted values of the detection sensitivities are equal within 5%. The reason is that the rate coefficient k_7 is essentially the same for the different RO_2 species, and radical-specific losses of RO_2 and RO by formation of organic nitrates and nitrites, respectively, play little role at the reduced instrumental pressure.

The relatively low RO_2 detection sensitivity for isobutane indicates a reduced HO_2 yield from the chemical RO_2 conversion. The likely reason is a more complex chain of conversion reactions. In the reaction of OH with isobutane, the H-atom abstraction occurs predominantly (70%) at the tertiary C–H site, yielding $(CH_3)_3CO_2$ as peroxy radical. The rate constant k_7 for reaction with NO is similar as that for smaller alkyl peroxy radicals. The resulting *tert*-butoxy

radical, however, has no H atom in the α position that could be abstracted by O_2 and form HO_2 . Rather, the alkoxy radical decomposes rapidly:⁴⁰

$$(CH_3)_3CO + M \rightarrow CH_3 + (CH_3)_2CO + M.$$
 (38)

The CH₃ fragment reacts with O₂ and produces a new peroxy radical, CH₃O₂, which has to undergo another reaction with NO to finally produce HO₂. Because of the additional reaction steps, the conversion of *tert*-butyl peroxy radicals to HO₂ is less complete within the available reaction time than that for for light n-alkyl peroxy radicals. A model calculation predicts a 34% smaller yield than that for an initially the same amount of CH₃O₂, which can explain much of the experimentally observed difference (Table III). More generally, alkoxy radicals of large alkanes ($>C_4$) have the tendency to decompose (or isomerize) in competition to the reaction with O₂.⁴⁰ Thus, large alkyl peroxy radicals may generally have a reduced detection sensitivity compared to CH₃O₂.

The reaction of ethene with OH yields β -hydroxyethyl peroxy radicals, $CH_2(OH)CH_2O_2$. The corresponding alkoxy radicals react mostly (78%) with O_2 and form directly HO_2 , whereas a smaller part (22%) first decomposes to the α -hydroxy radical $CH_2(OH)$, which is rapidly converted to HO_2 by the reaction with oxygen: 40,42

$$CH_2(OH)CH_2O + M \rightarrow CH_2(OH) + HCHO + M,$$
 (39)

$$CH_2(OH) + O_2 \rightarrow HCHO + HO_2.$$
 (40)

As for the small alkyl peroxy radicals (C_1-C_3) , the RO_2 to HO_2 conversion is rate limited by reaction (7), which has again the same rate coefficient (Table I). Thus, the detection sensitivity for the peroxy radicals of ethene is expected to be the same as that for CH_3O_2 , which agrees with the observations (Table III). The same kind of behavior is expected for β -hydroxyalkyl peroxy radicals from larger acyclic alkenes (C_2-C_5) . Here, the corresponding β -hydroxyalkoxy radicals decompose predominantly and yield α -hydroxyalkyl radicals, RC(OH)R', which produce HO_2 in a fast reaction with O_2 .

The 2-methyl-1,3-butadiene (isoprene) forms six RO_2 isomers in the reaction with OH. The rate coefficient of the RO_2 reaction with NO is the same as that for CH_3O_2 .⁴³ The main pathways of the formed alkoxy radicals are decomposition or isomerization reactions, which are all followed by rapid production of one HO2 radical for each alkoxy radical. Thus, isoprene hydroxylalkyl peroxy radicals are expected to have a similar detection sensitivity as methyl peroxy radicals. The measured value, however, is higher (21%), more than can be explained by the experimental errors. A possible reason would be a larger RO₂ production in the calibration source than is calculated. In principle, additional organic radicals can be formed by the 185 nm photolysis of isoprene, which is known to photodissociate at wavelengths below 255 nm. 44 However, the absorption cross section, which is of the order of 10⁻¹⁷ cm², ^{45,46} and the gasphase concentration of isoprene are two to three orders of magnitude too small in order to compete with the radical production by water-vapor photolysis. If the radical source is

^bNormalized to the value measured for CH₃O₂.

^cError bars are 1σ standard deviations.

^dSix isomers, see, e.g., Ref. 40.

not responsible, the enhanced sensitivity may be an indicator that the RO_2 to HO_2 conversion is more efficient than predicted by the known chemical mechanism.

F. Interferences

Some perturbation of the flow-reactor chemistry can be expected if the sampled ambient air is highly polluted. The influence of ambient NO, for example, which adds to the concentration of the injected NO reagent, can be estimated from Fig. 4 and has only a small influence on the detection sensitivity of RO_2 and HO_2 , of about +0.04% and -0.01% per ppbv NO, respectively. In the HOx mode, when the addition of NO reagent is turned off, the influence of ambient NO on the HO₂ detection is also small. However, the conversion of sampled RO₂ by ambient NO can make a significant contribution, presenting an interference for the HO2 measurement in the HOx mode with a relative efficiency of $C_{\text{CH}_2\text{O}_2}$: C_{HO_2} =2×10⁻³ per ppbv of ambient NO. The interference would thus exceed 5% for equal amounts of atmospheric RO2 and HO2 if the NO level becomes higher than 25 ppbv NO.

Atmospheric pollutants such as NO₂, CO, and hydrocarbons have very little impact on the measured peroxy-radical signals because the radical chemistry in the reactor is predominantly controlled by the reagent gases (CO, NO). A potential source of interference, however, is the thermal decomposition of atmospheric peroxy nitrates, which release peroxy radicals when the sampled air is expanded into the low-pressure flow reactor. Prominent species are HO₂NO₂ (pernitric acid, PNA) and CH₃O₂NO₂ (methyl peroxy nitrate, MePN), which are formed in an equilibrium that is established within seconds under typical boundary-layer conditions:⁴⁷

$$RO_2 + NO_2 + M \rightleftharpoons RO_2NO_2 + M.$$
 (41)

The atmospheric ratios $[RO_2NO_2]/[RO_2]$ can be estimated from $K_{\rm eq}[NO_2]$ using the published equilibrium constants $K_{\rm eq}(298~{\rm K})=1.6\times 10^{-11}~{\rm cm}^3$ for PNA and $2.7\times 10^{-12}~{\rm cm}^3$ for MePN. The resulting atmospheric peroxy nitrates are estimated to produce an interference, which is modeled to be 1.7% and 6% of the measured HO₂ and CH₃O₂ concentrations, respectively, assuming an ambient concentration of 10 ppbv of NO₂. Another important air pollutant that can decompose in the reactor is peroxy acetyl nitrate (PAN). The unimolecular decay of PAN, however, is slow $[k=2.6\times 10^{-4}~{\rm s}^{-1}$ at 25 hPa and 298 K (Ref. 48)], producing an interference equivalent of only 0.1 pptv RO₂ per ppbv of PAN.

Small interferences, which come from laser-generated OH in the LIF detection chamber, have been experimentally found. Ambient ozone as well as the NO added in the LIF chamber produce small OH signals with a quadratic laser-power dependence. The laser-power dependence suggests that one photon is required for photolytical OH generation and a second photon for detection of the generated OH. The NO interference is probably caused by HONO photolysis, which is possibly formed heterogeneously in the detection system. The size of this interference is equivalent to a peroxy-radical concentration of approximately 0.3 pptv and

is routinely subtracted for correction of the measured radical signals. The other interference can be explained by laser photolysis of O_3 [reactions (5) and (6)]. The interference is equivalent to about 0.1 pptv RO_2 per 100 ppbv O_3 in the presence of 0.7% water vapor and 25 mW laser power for the present instrument.

G. Limit of detection

The precision of the measured ROxLIF signals is limited by the shot noise of the photon counting. In the on-resonance mode there is a contribution from (1) the OH fluorescence of converted peroxy radicals, (2) the PMT dark signal (<0.1 counts s⁻¹), (3) a laser-excited nonresonant background signal $S_{\rm lb}$ (typically 20 counts s⁻¹), and (4) the lasergenerated NO interference $S_{\rm NO}$ (~25 counts s⁻¹) at an UV laser power of 25 mW. The off-resonance signal is equal to the nonresonant background signal plus the PMT dark signal only. Solar stray light contributions²⁵ play no role as the inlet nozzle of the fluorescence detection chamber is shielded by the flow reactor against incident solar radiation.

The radical signals are then determined by subtracting the off-resonance signal and the NO interference signal from the on-resonance signal. The limit of detection (LOD) of the resulting signal is ²⁰

$$LOD \approx SNR \sqrt{\left(\frac{1}{\Delta t_{on}} [S_{lb} + S_{NO}] + \frac{1}{\Delta t_{off}} S_{lb}\right)}.$$
 (42)

Here, $\Delta t_{\rm on}$ and $\Delta t_{\rm off}$ are the integration times for photon counting in the on- and off-resonance modes, respectively, and SNR is the signal-to-noise ratio. For the ROxLIF instrument, the signal LOD is equal to 3.2 counts s⁻¹ at 30 s of integration time (on and off resonances, each) and a SNR = 2, equivalent to about 0.05 pptv of RO_x or HO_x .

The concentration for RO_2 can be determined by subtracting the concentration of HO_x from RO_x . Likewise, HO_2 can be determined by subtracting the measured concentration of OH from HO_x . The resulting LODs for RO_2 and HO_2 are in the order of 0.1 pptv.

VII. AMBIENT AIR MEASUREMENT

First ambient air measurements were performed by the ROxLIF instrument in summer 2005 at the research center in Juelich, Germany. The site is surrounded by a forest and is situated in an area dominated by agriculture and strip mining. The LIF instrument was placed on a platform with its sampling inlet at 3.5 m above ground. The instrument was operated using the ROxLIF channel for alternating measurement of RO_x and HO_x , and a second channel was employed for concurrent measurement of OH. Concentrations of RO_2 and HO_2 were determined from the measured quantities, assuming that RO_2 is detected with the sensitivity of CH_3O_2 .

Figure 6 shows an example of diurnal profiles of peroxy radicals that were recorded on a mostly sunny day. The variations in RO_2 and HO_2 are highly correlated and the mixing ratios are of similar magnitude. The photochemically formed radicals reach the highest values when the solar actinic flux, represented by the photolysis frequency $j(NO_2)$ in Fig. 6, is at its daily maximum and the concentration of NO,

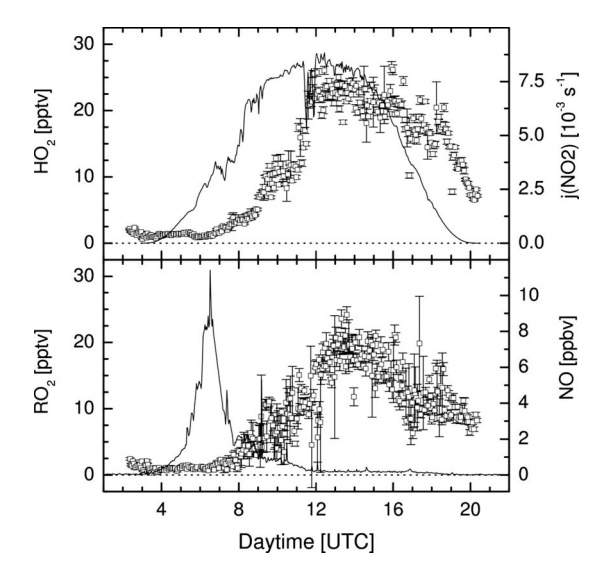


FIG. 6. In situ measurement of atmospheric mixing ratios of peroxy radicals (open symbols) with 1σ precision error bars and of NO (solid line, lower panel). The photolysis frequency $j(NO_2)$ is shown as a solid line in the upper panel. The measurements were obtained on 14 July 2005 in Juelich.

the main reactant of peroxy radicals, has become small. The lowest values of RO_2 and HO_2 are observed in the morning, when NO shows a high morning peak. Only after the decline of the high NO level the peroxy radicals start to increase and reach maximum values of about 20 pptv shortly after midday. Relatively high concentrations persist in the afternoon and even after sunset, indicating the possible existence of a nighttime radical source. These diurnal patterns are similar to what have been reported for peroxy radicals in other rural and urban environments. $^{50-52}$

The error bars in Fig. 6 represent 1σ precisions of the data points and are relatively small in most cases. The temporal variability in the peroxy radicals often exceeds the size of the error bars, indicating natural fluctuations of the RO₂ and HO₂ concentrations on a short time scale. Some error bars are notably large, for example, for RO2 at 12 coordinated universal time (UTC). The reason is that RO_2 is determined as the difference in RO_x and HO_x , which were measured in an alternating mode. Thus, whenever HO_x undergoes a relative large change between two adjacent measurements, the difference between ROx and HOx concentrations has a relatively large uncertainty, which increases the error bar. This situation could be improved by setting up a three-channel instrument, which records simultaneously OH and HO₂, as described, for example, in Ref. 25 and concurrently measures RO_x by a separate ROxLIF channel.

VIII. SUMMARY

The low-pressure LIF technique has been extended to enable the highly sensitive measurement of RO_2 besides the well established measurement of OH and HO_2 . The new method employs a two-stage chemical conversion scheme at a reduced pressure. In the first step organic peroxy radicals are transformed to HO_2 in a differentially pumped flow reactor. This is followed by chemical conversion of HO_2 to OH in a downstream low-pressure chamber, in which the result-

ing OH is detected by LIF at 308 nm. This concept has the advantage that the conditions for the radical conversion and detection can be independently optimized.

In the flow reactor a large excess of reagent gases (CO, NO) is applied to convert RO_2 into HO_2 . The added NO is responsible for the conversion of RO_2 to HO_x , while a large amount of CO shifts almost all HO_x to HO_2 , thus avoiding major radical losses by OH reactions, for example, with the reactor wall. The reduced pressure in the reactor slows down unwanted gas-phase reactions and minimizes the effect of radical losses such as recombination reactions of RO_x species with NO and interferences by ambient pollutants. The conditions in the LIF detection chamber are chosen to maximize the yield of laser-induced OH fluorescence per HO_2 collected from the flow reactor. This includes the further increase in NO for complete HO_2 to OH conversion and further lowering in the total pressure to reduce the collisional quenching of the excited OH fluorescence.

The quantitative method of water-vapor photolysis at 185 nm, which is widely used by various research groups for calibration of OH and HO₂ instruments, has been adopted to calibrate the sensitivity of the instrument. RO₂ radicals are generated by quantitative conversion of OH with a suitable hydrocarbon added to the calibration gas.

The new ROxLIF technique was characterized with respect to its detection sensitivity, the possible influence of instrumental parameters, and possible interferences by ambient trace gases. The ROxLIF instrument has a very high detection sensitivity, which results in low detection limits of about 0.1 pptv of RO_2 and HO_2 at a measurement time of 1 min per data point. The instrument has the ability to measure RO_2 radical species from simple alkanes, from monoalkenes, and from the most important biogenic hydrocarbon, isoprene, with almost the same sensitivity. The detection sensitivity was found to be higher than that expected for radicals from isoprene and might be smaller for large alkyl peroxy radicals but both need to be investigated by further experiments.

Interferences by ambient gases are generally small but require some consideration in polluted air with high NO_x levels above 20 ppbv. Atmospheric water vapor has a general influence, reducing the detection signals for peroxy radicals by about 10% over a range of mixing ratios of 0%–1% H_2O . This effect can be quantitatively explained by a fluorescence-quenching model of laser-excited OH and measurements can be easily corrected in the data evaluation.

First ambient air measurements were performed in summer 2005 showing reasonable diurnal profiles of peroxy radicals. ROxLIF was also successfully compared with the well established MI-ESR technique. The results of this comparison will be reported elsewhere. Based on its ability and performance, the new measurement technique for RO_2 and HO_2 is expected to provide improved understanding of the fast radical chemistry in the troposphere in future field campaigns.

ACKNOWLEDGMENTS

We thank M. Mihelcic and F. Rohrer for helpful discussions, R. Wegener for providing isoprene gas mixtures for

- ¹R. Atkinson and J. Arey, Chem. Rev. (Washington, D.C.) **103**, 4605 (2003).
- ²D. H. Ehhalt, Phys. Chem. Chem. Phys. 1, 5401 (1999).
- ³D. Mihelcic, P. Müsgen, and D. H. Ehhalt, J. Atmos. Chem. 3, 341 (1985).
- ⁴D. Mihelcic, A. Volz-Thomas, H. W. Pätz, D. Kley, and M. Mihelcic, J. Atmos. Chem. 11, 271 (1990).
- ⁵C. A. Cantrell, D. H. Stedman, and G. J. Wendel, Anal. Chem. **56**, 1496 (1984).
- ⁶C. A. Cantrell, R. E. Shetter, and J. G. Calvert, Anal. Chem. 68, 4194 (1996).
- ⁷D. R. Hastie, M. Weissenmayer, J. P. Burrows, and G. W. Harris, Anal. Chem. **63**, 2048 (1991).
- ⁸ K. C. Clemitshaw, L. J. Carpenter, and S. A. Penkett, J. Geophys. Res. 102, 25405 (1997).
- ⁹ J. Burkert, M. D. Andrés Hernández, D. Stöbener, M. Weissenmayer, and A. Kraus, J. Geophys. Res. **106**, 5457 (2001).
- ¹⁰ Y. Sadanaga, A. Yoshino, K. Watanaba, A. Yoshioka, Y. Wakazono, Y. Kanaya, and Y. Kajii, Rev. Sci. Instrum. 75, 864 (2004).
- ¹¹C. M. Mihele and D. R. Hastie, J. Atmos. Ocean. Technol. **17**, 788 (2000).
- ¹² T. J. Green, C. E. Reeves, Z. L. Fleming, N. Brough, A. R. Rickard, B. J. Bandy, P. S. Monks, and S. A. Penkett, J. Environ. Monit. 8, 530 (2006).
- ¹³C. M. Mihele and D. R. Hastie, Geophys. Res. Lett. **25**, 1911 (1998).
- ¹⁴L. Reichert, M. D. Andrés Hernández, D. Stöbener, J. Burkert, and J. P. Burrows, J. Geophys. Res. **108**, 4017 (2003).
- ¹⁵T. Reiner, M. Hanke, and F. Arnold, J. Geophys. Res. **102**, 1311 (1997).
- ¹⁶M. Hanke, J. Uecker, T. Reiner, and F. Arnold, Int. J. Mass. Spectrom. 213, 91 (2002).
- ¹⁷ G. D. Edwards, C. A. Cantrell, S. Stephens, B. Hil, O. Goyea, R. E. Shetter, R. L. Mauldin, E. Kosciuch, D. J. Tanner, and F. L. Eisele, Anal. Chem. 75, 5317 (2003).
- ¹⁸T. M. Hard, R. J. O'Brien, C. Y. Chan, and A. A. Mehrabzadeh, Environ. Sci. Technol. **18**, 768 (1984).
- ¹⁹ P. S. Stevens, J. H. Mather, and W. H. Brune, J. Geophys. Res. **99**, 3543 (1994).
- ²⁰F. Holland, M. Heßling, and A. Hofzumahaus, J. Atmos. Sci. **52**, 3393 (1995).
- ²¹F. Holland, U. Aschmutat, M. Heßling, A. Hofzumahaus, and D. H. Ehhalt, J. Atmos. Chem. 31, 205 (1998).
- ²² D. J. Creasey, P. A. Halford-Maw, D. E. Heard, M. J. Pilling, and B. J. Whitaker, J. Chem. Soc., Faraday Trans. 93, 2907 (1997).
- ²³ Y. Kanaya, Y. Sadanaga, J. Hirokawa, Y. Kajii, and H. Akimoto, J. Atmos. Chem. 38, 73 (2001).
- ²⁴ D. E. Heard and M. J. Pilling, Chem. Rev. (Washington, D.C.) **103**, 5163 (2003).
- ²⁵ F. Holland, A. Hofzumahaus, J. Schäfer, A. Kraus, and H.-W. Pätz, J. Geophys. Res. **108**, 8246 (2003).
- ²⁶ E. Schlosser, B. Bohn, T. Brauers, H.-P. Dorn, H. Fuchs, R. Häseler, A. Hofzumahaus, F. Holland, F. Rohrer, L. O. Rupp, M. Siese, R. Tillmann, and A. Wahner, J. Atmos. Chem. 56, 187 (2007).
- ²⁷ U. Aschmutat, M. Heßling, F. Holland, and A. Hofzumahaus, in *Physico-Chemical Behaviour of Atmospheric Pollutants*, edited by G. Angeletti and G. Restelli (European Commission, Brussels, 1994), Vol. 2, pp. 811–816
- ²⁸ A. Hofzumahaus, U. Aschmutat, U. Brandenburger, T. Brauers, H.-P.

- Dorn, M. Hausmann, M. Heßling, F. Holland, C. Plass-Dülmer, and D. H. Ehhalt, J. Atmos. Chem. **31**, 227 (1998).
- ²⁹ M. Schultz, M. Heitlinger, M. Mihelcic, and A. Volz-Thomas, J. Geophys. Res. **100**, 18,811 (1995).
- ³⁰ A. Hofzumahaus, T. Brauers, U. Aschmutat, U. Brandenburger, H.-P. Dorn, M. Hausmann, M. Heßling, F. Holland, C. Plass-Dülmer, M. Sedlacek, M. Weber, and D. H. Ehhalt, Geophys. Res. Lett. 24, 3039 (1997).
- ³¹C. A. Cantrell, A. Zimmer, and G. S. Tyndall, Geophys. Res. Lett. 24, 2195 (1997).
- ³² D. J. Creasey, D. E. Heard, and J. D. Lee, Geophys. Res. Lett. 27, 1651 (2000).
- ³³ A. V. Ivanov, S. Trakhtenberg, A. K. Bertram, Y. M. Gershenzon, and M. J. Molina, J. Phys. Chem. A 111, 1632 (2007).
- ³⁴ V. B. Rozhenshtein, Y. M. Gershenzon, S. D. Il'in, O. P. Kishkovich, and R. T. Malkhasyan, Kinet. Catal. USSR 26, 460 (1985).
- ³⁵ A. E. Bailey, D. arE. Heard, D. A. Henderson, and P. H. Paul, Chem. Phys. Lett. **302**, 132 (1999).
- ³⁶ A. Hofzumahaus, U. Aschmutat, M. Heßling, F. Holland, and D. H. Ehhalt, Geophys. Res. Lett. 23, 2541 (1996).
- ³⁷C. M. Mihele and D. R. Hastie, Int. J. Chem. Kinet. **31**, 145 (1999).
- ³⁸D. E. Heard and D. A. Henderson, Phys. Chem. Chem. Phys. **2**, 67 (2000).
- ³⁹ N. I. Butkovskaya, A. Kukui, N. Pouvesle, and G. Le Bras, J. Phys. Chem. A 109, 6509 (2005).
- ⁴⁰R. Atkinson, J. Phys. Chem. Ref. Data **26**, 215 (1997).
- ⁴¹ F. P. Tully, J. E. M. Goldsmith, and A. T. Droege, J. Phys. Chem. **90**, 5932 (1986)
- ⁴²J. J. Orlando, G. S. Tyndall, M. Bilde, C. Ferronato, T. J. Wallington, L. Vereecken, and J. Peeters, J. Phys. Chem. A 102, 8116 (1998).
- ⁴³D. Zhang, R. Zhang, and S. W. North, J. Phys. Chem. A **107**, 11013 (2003)
- ⁴⁴ R. Demers, G. J. Collin, and H. Gagnon-Deslauriers, Can. J. Chem. **56**, 1864 (1978).
- ⁴⁵L. C. Jones and L. W. Taylor, Anal. Chem. 27, 228 (1955).
- ⁴⁶P. Campuzano-Jost, M. B. Williams, L. D. Ottone, and A. J. Hynes, J. Phys. Chem. A **108**, 1537 (2004).
- ⁴⁷ M. E. Jenkin and K. C. Clemitshaw, Atmos. Environ. **34**, 2499 (2000).
- ⁴⁸ S. P. Sander, R. R. Friedl, D. M. Golden, M. J. Kurylo, R. E. Huie, V. L. Orkin, G. K. Moortgat, A. R. Ravishankara, C. E. Kolb, M. J. Molina, P. H. Wine, and B. J. Finlayson-Pitts, "Chemical kinetics and photochemical data for use in atmospheric studies, evaluation number 14," NASA-JPL Publication No. 02-25, 2003.
- ⁴⁹G. P. Smith and D. R. Crosley, J. Geophys. Res. **95**, 16,427 (1990).
- ⁵⁰D. Mihelcic, F. Holland, A. Hofzumahaus, L. Hoppe, S. Konrad, P. Müsgen, H.-W. Pätz, H.-J. Schäfer, T. Schmitz, A. Volz-Thomas, K. Bächmann, S. Schlomski, U. Platt, A. Geyer, B. Alicke, and G. K. Moortgat, J. Geophys. Res. 108, 8254 (2003).
- ⁵¹ T. R. Shirley, W. H. Brune, X. Ren, J. Mao, R. Lesher, B. Cardenas, R. Volkammer, L. T. Molina, M. J. Molina, B. Lamb, E. Velasco, T. Jobson, and M. Alexander, Atmos. Chem. Phys. 6, 2753 (2006).
- ⁵² K. M. Emmerson, N. Carslaw, D. C. Carslaw, J. D. Lee, G. McFiggans, W. J. Bloss, T. Gravestock, D. E. Heard, J. Hopkins, T. Ingham, M. J. Pilling, S. C. Smith, M. Jacobs, and P. S. Monks, Atmos. Chem. Phys. 7, 167 (2007).
- ⁵³ J. Zhang, T. Dransfield, and N. M. Donahue, J. Phys. Chem. A **108**, 9082 (2004).